Journal of Sound and Vibration (2001) **256**(1), 131–153
doi:10.1006/jsvi.2001.4206, available online at http://www.idealibrary.com on IDEAL®

LINE FORCE RECEPTANCE OF AN ELASTIC CYLINDRICAL SHELL WITH HEAVY EXTERIOR FLUID LOADING

E. A. Skelton

Department of Mathematics, Imperial College of Science, Technology and Medicine, Huxley Building, 180 Queen's Gate, London SW7 2BZ, England. E-mail: e.skelton@ic.ac.uk

(*Received* 24 *July* 2001, *and in final form* 12 *November* 2001)

A time-harmonic line force is applied to an infinite elastic cylindrical shell immersed in compressible fluid. The force may also have axial harmonic dependence. The formal solution for the shell displacement is obtained as the sum of circumferential harmonics and evaluated in the asymptotic limit of heavy exterior fluid-loading. The resulting asymptotic expressions for the elements of the receptance matrix, either at the line of application of the force, or elsewhere on the shell surface, are simple trigonometric functions of the shell and fluid parameters, and show excellent agreement with numerical evaluation of the circumferential harmonic series over a wide frequency range.

1. INTRODUCTION

Many marine and aerospace structures can be modelled basically by elastic plates and cylindrical shells. The motion of the basic structure is then modified by the addition of other internal structures such as machinery, or ribs or struts to strengthen the structure. Much work has been carried out on the theory of the vibration of infinitely long cylindrical elastic shells. Greenspon [1] provides a useful survey of this work up to 1960. Warburton [2] included the effects of an acoustic medium. More recent work by Fuller and Fahy [3], Fuller [4] and Scott [5] has also investigated the vibration and acoustics of the fluid-loaded cylindrical shell. A feature of these papers is that because the shell geometry is axisymmetric the displacements, forces, pressures, etc. may all be expanded as Fourier series in the circumferential co-ordinate, and the shell equations are such that the different harmonics are uncoupled from each other.

With the addition of stiffening, or other structures, the reaction forces at the intersections of the stiffening and the original structure must be related to the displacement there, so that both displacements may be made equal and the reaction forces equal and opposite. One of the simplest geometries for this intersection is a line. Much theoretical work has been carried out on elastic plates with line constraints, for example references [6–9], which make use of this receptance method.

For cylindrical shells the effects of axisymmetric ring stiffeners have been addressed by many authors, for example references [10–12]. Wilken and Soedel [10] use the receptance method to analyze a ring-stiffened cylinder with no fluid-loading. Mead and Bardell [11] also consider cylinders with no fluid-loading, but use a variational method to calculate the forces. Skelton [12] has used the receptance method to calculate reaction forces when fluid-loading is included, and has also obtained results in the asymptotic limit of heavy

0022-460X/02/$35.00

exterior fluid-loading, which is appropriate to the case of thin steel shells in water at low frequencies, for example. In problems of this type, the axisymmetric geometry again ensures that the equations for each circumferential harmonic are uncoupled from those of the other harmonics.

Axially stiffened cylinders are also used in underwater vehicles and the aerospace industry, and these have been the subject of many investigations, for example references [13–21]. With an axial constraint, the geometry is no longer axisymmetric and hence the circumferential harmonics are coupled. Reddy and Mallik [13] considered periodic axial stiffeners and expanded the quantities as harmonic series considering the excitation by each harmonic in turn. Their solution, therefore, involves the numerical evaluation of several infinite series. Mead and Bardell [14] use the periodic nature of the stiffeners to find eigenvalues for an in vacuo shell with sinusoidal variation along the shell. Their method does not involve receptance evaluations, but requires corresponding infinite sum evaluations. Bjarnason *et al.* [15] use the Lagrange equation formulation to investigate a shell with an internal plate, variously attached to it, immersed in fluid. Their method also involves numerical calculation of the shell mobility (related to the receptance) from an infinite series. More recently, a series of papers [16–20] by Guo investigated various acoustic scattering and radiation problems related to an infinite elastic cylindrical shell, immersed in fluid, with two axial line constraints due to the attachment of an internal elastic plate, or a mass–spring system. These use the receptance method and require numerical evaluation of infinite summations to calculate the receptances of the shell. A similar geometry, but with the plate located on a diameter, was considered by Baillard *et al.* [21], who used elasticity theory to model the shell, and successfully compared their results both with those obtained from shell theory and experimentally.

Thus, the subject of infinite elastic cylindrical shells with axial line constraints may be seen to be an active research area with practical applications. In this paper the (3×3) receptance matrix for the cylindrical shell relating the radial, axial and circumferential displacement components to the corresponding components of a line force applied parallel to the axis of the shell are derived. The applied line force may have $\exp(i\alpha z)$ variation, corresponding to the type of reaction force expected in the case of an obliquely incident acoustic wave, for example. The elements of the receptance matrix, which are in the form of infinite series, are then evaluated asymptotically in the limit of heavy exterior fluid-loading, which is appropriate to the practical case of a steel shell in water at low frequencies, for example. The resulting asymptotic expressions for the receptance elements, either at the force application line or elsewhere on the shell surface, are simple trigonometric functions of the shell and fluid parameters, which show excellent agreement with numerical results over a wide frequency range. These results may, therefore, be used both to avoid evaluating the infinite summations, which may converge slowly, and to interpret subsequent results.

2. EQUATIONS OF MOTION OF THE LINE-EXCITED SHELL

It is natural to use the usual cylindrical polar co-ordinate system, (r, z, ϕ), to analyze this problem in cylindrical geometry. A time-harmonic line force, whose amplitude may depend on the axial location, z, is applied to the shell at some constant value of ϕ, $\phi = \phi_0$. Since the co-ordinate axes may be rotated if necessary it is sufficient to consider only the case $\phi_0 = 0$. The displacement of the cylindrical elastic shell is assumed to satisfy the Donnell–Mushtari equations of motion, for which the effects of rotary inertia are neglected. Hence, the equations of motion for the shell may be obtained as (see, for example the book

by Junger and Feit [22])

$$\frac{\sigma}{a}\frac{\partial u_z}{\partial z}+\frac{1}{a^2}\frac{\partial u_\phi}{\partial \phi}+\frac{u_r}{a^2}+\beta^2\left[a^2\frac{\partial^4 u_r}{\partial z^4}+2\frac{\partial^4 u_r}{\partial z^2\partial \phi^2}+\frac{1}{a^2}\frac{\partial^4 u_r}{\partial \phi^4}\right]+\frac{\rho_s(1-\sigma^2)}{E}\frac{\partial^2 u_r}{\partial t^2}$$

$$=(1-\sigma^2)[F_r(z,t)\delta(\phi)-p_e(a,z,\phi)]/Eh, \tag{1}$$

$$\frac{\partial^2 u_z}{\partial z^2}+\frac{(1-\sigma)}{2a^2}\frac{\partial^2 u_z}{\partial \phi^2}+\frac{(1+\sigma)}{2a}\frac{\partial^2 u_\phi}{\partial \phi \partial z}+\frac{\sigma}{a}\frac{\partial u_r}{\partial z}-\frac{\rho_s(1-\sigma^2)}{E}\frac{\partial^2 u_z}{\partial t^2}$$

$$=-(1-\sigma^2)F_z(z,t)\delta(\phi)/Eh, \tag{2}$$

$$\frac{(1+\sigma)}{2a}\frac{\partial^2 u_z}{\partial \phi \partial z}+\frac{(1-\sigma)}{2}\frac{\partial^2 u_\phi}{\partial z^2}+\frac{1}{a^2}\frac{\partial^2 u_\phi}{\partial \phi^2}+\frac{1}{a^2}\frac{\partial u_r}{\partial \phi}-\frac{\rho_s(1-\sigma^2)}{E}\frac{\partial^2 u_\phi}{\partial t^2}$$

$$=-(1-\sigma^2)F_\phi(z,t)\delta(\phi)/Eh, \tag{3}$$

in which a is the mean radius of the shell, h is its thickness, $\beta^2=h^2/12a^2$, E, σ and ρ_s are, respectively, Young's modulus, the Poisson ratio and the density of the shell material, $p_e(a,z,\phi)$ is the acoustic pressure in the exterior fluid and $F_r(z,t)\delta(\phi)$, $F_z(z,t)\delta(\phi)$ and $F_\phi(z,t)\delta(\phi)$ represent the force per unit area applied to the shell in the radial, axial and circumferential directions.

In this problem it will be assumed that the applied forces are all time-harmonic, with radian frequency ω, and that the axial variation of each of the applied forces, and hence of all the other quantities is $\exp(i\alpha z)$, where α is a constant which may be proportional to the excitation frequency. Thus, for example,

$$F_r(z,t)=F_r\exp(i\alpha z-i\omega t). \tag{4}$$

The exponential factor $\exp(-i\omega t)$ will be omitted from all subsequent equations.

The pressure in the exterior fluid is an outgoing wave solution of the reduced wave equation

$$(\nabla^2+k^2)p_e(r,z,\phi)=0, \quad r>a, \tag{5}$$

where $k=\omega/c$ is the acoustic wavenumber in the exterior fluid in which the sound speed is c, and which satisfies the boundary condition of continuity of radial displacement at the shell surface, $r=a$,

$$\left.\frac{\partial p_e}{\partial r}\right|_{r=a}=\rho\omega^2 u_r, \tag{6}$$

where ρ is the density of the exterior fluid.

It is convenient in this cylindrical geometry to express the shell displacements, acoustic pressure and the applied forces as Fourier series with respect to the circumferential co-ordinate ϕ. The $\delta(\phi)$ function which occurs in each of the applied force terms may thus be expanded as

$$\delta(\phi)=\frac{1}{2\pi}\sum_{n=0}^{\infty}e_n\cos n\phi, \tag{7}$$

where $e_0 = 1$, and $e_n = 2$ for $n \geqslant 1$, and the shell displacements may be written in the form

$$\begin{pmatrix} u_r(z,\phi) \\ u_z(z,\phi) \\ u_\phi(z,\phi) \end{pmatrix} = \mathrm{e}^{\mathrm{i}\alpha z} \sum_{n=0}^{\infty} \begin{pmatrix} u_{rn} \cos n\phi + v_{rn} \sin n\phi \\ u_{zn} \cos n\phi + v_{zn} \sin n\phi \\ u_{\phi n} \sin n\phi - v_{\phi n} \cos n\phi \end{pmatrix}, \tag{8}$$

from which it follows that the exterior pressure is

$$p_e(r,z,\phi) = \rho\omega^2 \mathrm{e}^{\mathrm{i}\alpha z} \sum_{n=0}^{\infty} (u_{rn} \cos n\phi + v_{rn} \sin n\phi)\, \mathrm{H}_n(\gamma r)/\gamma \mathrm{H}_n'(\gamma a), \tag{9}$$

where $\gamma = \sqrt{k^2 - \alpha^2}$, and $\mathrm{H}_n = \mathrm{J}_n + \mathrm{i}\mathrm{Y}_n$ is the Hankel function of the first kind where J_n and Y_n are Bessel functions of the first and second kinds, respectively, which is the outgoing wave solution of the reduced wave equation (5) which satisfies the boundary condition (6).

By substituting these expressions for the displacements, pressure and forcing terms into the equations of motion (1)–(3) for the shell, the following matrix equations relating the shell displacement components for each harmonic to the applied forces are obtained:

$$\mathbf{S}(\alpha, n) \begin{pmatrix} u_{rn} \\ u_{zn} \\ u_{\phi n} \end{pmatrix} = e_n \begin{pmatrix} F_r \\ F_z \\ 0 \end{pmatrix}, \tag{10}$$

$$\mathbf{S}(\alpha, n) \begin{pmatrix} v_{rn} \\ v_{zn} \\ v_{\phi n} \end{pmatrix} = e_n \begin{pmatrix} 0 \\ 0 \\ -F_\phi \end{pmatrix}, \tag{11}$$

where

$$S_{11} = E_1[1/a^2 + \beta^2(a^2\alpha^4 + 2n^2\alpha^2 + n^4/a^2)] - \rho_s\omega^2 h + \rho\omega^2 \mathrm{H}_n(\gamma a)/\gamma \mathrm{H}_n'(\gamma a), \tag{12a}$$

$$S_{12} = E_1 \mathrm{i}\alpha\sigma/a, \quad S_{13} = E_1 n/a^2, \quad S_{21} = -S_{12}, \tag{12b–d}$$

$$S_{22} = E_1[\alpha^2 + n^2(1-\sigma)/2a^2] - \rho_s\omega^2 h, \quad S_{23} = -E_1 \mathrm{i}\alpha n(1+\sigma)/2a, \tag{12e, f}$$

$$S_{31} = S_{13}, \quad S_{32} = -S_{23}, \quad S_{33} = E_1[\alpha^2(1-\sigma)/2 + n^2/a^2] - \rho_s\omega^2 h, \tag{12g–i}$$

in which $E_1 = Eh/(1-\sigma^2)$. Hence, inverting these equations and rearranging the terms

$$\begin{pmatrix} u_{rn} \cos n\phi + v_{rn} \sin n\phi \\ u_{zn} \cos n\phi + v_{zn} \sin n\phi \\ u_{\phi n} \sin n\phi - v_{\phi n} \cos n\phi \end{pmatrix} = e_n \begin{pmatrix} S_{11}^{-1} \cos n\phi & S_{12}^{-1} \cos n\phi & -S_{13}^{-1} \sin n\phi \\ S_{21}^{-1} \cos n\phi & S_{22}^{-1} \cos n\phi & -S_{23}^{-1} \sin n\phi \\ S_{31}^{-1} \sin n\phi & S_{32}^{-1} \sin n\phi & S_{33}^{-1} \cos n\phi \end{pmatrix} \begin{pmatrix} F_r \\ F_z \\ F_\phi \end{pmatrix} \tag{13}$$

and thus from equation (8) the shell displacements may be related to the applied line forces

$$\begin{pmatrix} u_r(z,\phi) \\ u_z(z,\phi) \\ u_\phi(z,\phi) \end{pmatrix} = \mathrm{e}^{\mathrm{i}\alpha z} \mathbf{A}(\alpha, \phi) \begin{pmatrix} F_r \\ F_z \\ F_\phi \end{pmatrix}, \tag{14}$$

where the (3×3) receptance matrix $\mathbf{A}(\alpha, \phi)$ is

$$\boldsymbol{A}(\alpha, \phi) = \sum_{n=0}^{\infty} e_n \begin{pmatrix} S_{11}^{-1} \cos n\phi & S_{12}^{-1} \cos n\phi & -S_{13}^{-1} \sin n\phi \\ S_{21}^{-1} \cos n\phi & S_{22}^{-1} \cos n\phi & -S_{23}^{-1} \sin n\phi \\ S_{31}^{-1} \sin n\phi & S_{32}^{-1} \sin n\phi & S_{33}^{-1} \cos n\phi \end{pmatrix}. \tag{15}$$

In these, and all subsequent equations, the notation S_{ij}^{-1} is used to mean $(\mathbf{S}^{-1})_{ij}$, i.e., the ijth element of the inverse of the matrix $\mathbf{S}$. In the general case the elements of $\mathbf{A}(\alpha, \phi)$ may be evaluated numerically, by truncating the infinite sum at a suitably large finite number. In the next section they will be evaluated asymptotically for the limiting case of heavy exterior fluid-loading, which is appropriate to many practical underwater structures over a substantial range of low frequencies. It may also be noted here that the shell mobility [4, 15] relates the velocity components to the applied force components. Hence for the time-harmonic oscillations considered here the mobility matrix is $-\mathrm{i}\omega\mathbf{A}$.

3. ASYMPTOTIC EVALUATION OF THE RECEPTANCE MATRIX FOR HEAVY EXTERIOR FLUID-LOADING

Before evaluating the infinite sums of equation (15) asymptotically it is convenient to make the following definitions, as in reference [12]:

$$D = E_1 \beta^2 a^2, \quad \alpha_1 = (\rho\omega^2/D)^{1/5}, \quad \alpha_0 = (\rho_s \omega^2 h/D)^{1/4}. \tag{16–18}$$

Here D is the bending stiffness of a plate with the same thickness as the shell, α_1 is the fluid-loaded free wavenumber of such a plate in the heavy fluid-loading limit, and α_0 is the *in vacuo* free wavenumber of the plate. Heavy fluid-loading means here, as in the plate case [9], that

$$\alpha_1 \gg \alpha_0, \quad \text{and} \quad \alpha_1 \gg k. \tag{19, 20}$$

These heavy fluid-loading requirements can also be expressed in terms of the density of the exterior fluid: ρ must be large compared to both of $\rho_s h(\rho_s \omega^2 h/D)^{1/4}$ and $\omega^3 D/c^5$. They may also be expressed in terms of the frequency: ω must be small compared to both $(\rho/\rho_s h)^2 (D/\rho_s h)^{1/2}$ and $(\rho c^5/D)^{1/3}$.

Although not linked to the heavy fluid-loading requirement it may also be noted here that only the case when

$$\alpha \leqslant k \quad \text{and hence } \gamma \leqslant k \tag{21, 22}$$

is considered here.

In the analysis which follows, the leading order term of each element of $\mathbf{A}(\alpha, \phi)$ will be evaluated separately in the asymptotic limit of heavy fluid loading. For example, noting that

$$S_{11}^{-1} = (S_{22}S_{33} - S_{23}S_{32})/\Delta, \tag{23}$$

where $\Delta(\alpha, n)$ is the determinant of the matrix $\mathbf{S}(\alpha, n)$,

$$\Delta = S_{11}(S_{22}S_{33} - S_{23}S_{32}) - S_{12}(S_{21}S_{33} - S_{23}S_{31}) + S_{13}(S_{21}S_{32} - S_{22}S_{31}), \tag{24}$$

it is clear that as $\rho \to \infty$, for fixed values of n and α, the leading order term of S_{11}^{-1} is proportional to an $O(1/\rho)$ term, or equivalently to an $O(1/\alpha_1^5)$ term. Thus, any sum over a finite range of n will also have this behaviour. Hence, the asymptotic form of any infinite sums in the asymptotic limit of heavy fluid-loading may be obtained by replacing the

summand by its form for large n, which is inaccurate only over a finite, ρ-independent, range of n and thus leads to a correction which is $O(1/\rho)$.

By making use of the expressions (12) for the elements of **S** it is clear that, for large values of n, Δ may be written as

$$\Delta = (S_{22}S_{33} - S_{23}S_{32})\left\{\left(S_{11} - \frac{E_1}{a^2}\right) + O\left(\frac{1}{n^2}\right)\right\}. \tag{25}$$

By using the asymptotic form for large order Hankel functions given in, for example reference [23],

$$\mathrm{H}_n(\xi) \sim -\mathrm{i}\sqrt{\frac{2}{\pi n}}\left(\frac{\mathrm{e}\xi}{2n}\right)^{-n} \quad \text{as } n \to \infty, \tag{26}$$

the expression involving Hankel functions in the S_{11} element may be approximated when $n > \gamma a$, as

$$\rho\omega^2\mathrm{H}_n(\gamma a)/\gamma\mathrm{H}_n'(\gamma a) \sim -\rho\omega^2 a/n, \tag{27}$$

allowing the element of the inverse, S_{11}^{-1} to be approximated for large n as

$$S_{11}^{-1} \sim \frac{a^4}{D\{(n^2 + (\alpha a)^2)^2 - (\alpha_0 a)^4 - (\alpha_1 a)^5/n\}}. \tag{28}$$

Further approximation when $\alpha \ll \alpha_1$ and $\alpha_0 \ll \alpha_1$ allows this to be written as

$$S_{11}^{-1} \sim \frac{a^4 n}{D(n^5 - (\alpha_1 a)^5)}. \tag{29}$$

Thus

$$A_{11}(\alpha,\phi) \sim \frac{a^4}{D}\left\{\sum_{n=0}^{\infty}\frac{e_n n\cos n\phi}{(n^5 - (\alpha_1 a)^5)} + O\left(\frac{1}{(\alpha_1 a)^5}\right)\right\}. \tag{30}$$

It remains therefore to evaluate this infinite sum in the limit of large $\alpha_1 a$. This may be accomplished by rearranging it as

$$\sum_{n=0}^{\infty}\frac{e_n n\cos n\phi}{(n^5 - (\alpha_1 a)^5)} = \sum_{n=0}^{\infty}\frac{e_n n\cos n|\phi|}{(n^5 - (\alpha_1 a)^5)} = \sum_{n=-\infty}^{\infty}\frac{|n|\mathrm{e}^{\mathrm{i}n|\phi|}}{(|n|^5 - (\alpha_1 a)^5)}, \tag{31}$$

and then making use of the Poisson summation theorem to facilitate evaluation of the sum. The Poisson summation theorem states that (see, for example reference [24]):

If $g(x)$ is continuous and of bounded variation on $(-\infty, \infty)$ and tends to 0 as $|x| \to \infty$ such that $\int_{-\infty}^{\infty} g(x)\mathrm{d}x$ converges, then

$$\sum_{m=-\infty}^{\infty} g(\lambda m) = \frac{1}{\lambda}\sum_{n=-\infty}^{\infty} G(2n\pi/\lambda) \tag{32}$$

where $G(s)$ is the Fourier transform of $g(x)$,

$$G(s) = \int_{-\infty}^{\infty} g(x)\mathrm{e}^{-\mathrm{i}sx}\mathrm{d}x. \tag{33}$$

The function defined as

$$g(x) = \frac{|x|\mathrm{e}^{\mathrm{i}x|\phi|}}{(|x|^5 - (\alpha_1 a)^5)} \tag{34}$$

satisfies all the requirements stated in the Poisson summation theorem, above, when the small amount of damping in the shell is included, and with $\lambda = 1$ the left-hand side of equation (32) is the sum required in equation (31). Thus,

$$\sum_{n=0}^{\infty} \frac{e_n n \cos n\phi}{(n^5 - (\alpha_1 a)^5)} = \sum_{n=-\infty}^{\infty} G(2n\pi), \tag{35}$$

where

$$G(s) = \int_0^{\infty} \frac{x(e^{-i|s-|\phi||x} + e^{i|s-|\phi||x})}{(x^5 - (\alpha_1 a)^5)} dx. \tag{36}$$

When the arguments of the exponentials in the integrand above are zero, the integral may be evaluated exactly using contour integration, by closing the contour with an arc at infinity subtending an angle $2\pi/5$ at the origin, and returning to the origin along the straight line to close the contour, thus enclosing only a single pole at $x = \alpha_1 a$. Thus,

$$G(|\phi|) = \frac{2\pi}{5(\alpha_1 a)^3}(i - \cot(2\pi/5)). \tag{37}$$

For $s \neq |\phi|$ the integral in equation (36) is regarded as the sum of two terms which are treated separately. The integration contour for the first integral is closed by an arc in the lower half-plane, returning to the origin along the negative imaginary axis. This contour encloses only the pole located at $\alpha_1 a \exp(-2i\pi/5)$. Thus,

$$\int_0^{\infty} \frac{x e^{-i|s-|\phi||x}}{(x^5 - (\alpha_1 a)^5)} dx = \frac{2\pi i}{5(\alpha_1 a)^3} [e^{6i\pi/5} e^{-i|s-|\phi||\alpha_1 a(\cos(2\pi/5) - i\sin(2\pi/5))}] + \int_0^{-i\infty} \frac{z e^{-i|s-|\phi||z}}{(z^5 - (\alpha_1 a)^5)} dz. \tag{38}$$

The integrand on the right-hand side of equation (38) decays exponentially with z and so only the contribution to the integral near to 0 will be significant. This, however, is $O(1/(\alpha_1 a)^5)$ and is thus of the order of terms which have already been neglected, so this will also be neglected. The pole contribution is exponentially small as $\alpha_1 a \to \infty$ and will also therefore be neglected here. The integration contour for the second integral of equation (36) may be closed by the corresponding contour in the upper half-plane. Hence

$$\int_0^{\infty} \frac{x e^{i|s-|\phi||x}}{(x^5 - (\alpha_1 a)^5)} dx = \frac{2\pi i}{5(\alpha_1 a)^3} [e^{i|s-|\phi||\alpha_1 a} + e^{-6i\pi/5} e^{i|s-|\phi||\alpha_1 a(\cos(2\pi/5) + i\sin(2\pi/5))}] + \int_0^{i\infty} \frac{z e^{i|s-|\phi||z}}{(z^5 - (\alpha_1 a)^5)} dz. \tag{39}$$

Combining these results, the leading order terms are found to be,

$$G(s) \sim \frac{2\pi i}{5(\alpha_1 a)^3} e^{i|s-|\phi||\alpha_1 a} \quad \text{as} \quad \alpha_1 a \to \infty,\ s \neq |\phi|. \tag{40}$$

Hence,

$$\sum_{n=-\infty}^{\infty} G(2n\pi) \sim G(0) + \frac{2\pi i}{5(\alpha_1 a)^3}(e^{i|\phi|\alpha_1 a} + e^{-i|\phi|\alpha_1 a}) \sum_{n=1}^{\infty} e^{2in\pi\alpha_1 a}, \quad |\phi| < 2\pi, \tag{41}$$

in which, if $\phi = 0$, the value of $G(0)$ is given by equation (37), and if $\phi \neq 0$ it is given by equation (40). After noting that the infinite sum remaining on the right-hand side of

equation (41) is a geometric progression, whose sum is therefore well known, and some simplification of the resulting expressions it can be shown that

$$\sum_{n=0}^{\infty} \frac{e_n n \cos n\phi}{n^5 - (\alpha_1 a)^5} \sim \begin{cases} \dfrac{-2\pi}{5(\alpha_1 a)^3}\left\{\cot\left(\dfrac{2\pi}{5}\right) + \cot(\pi\alpha_1 a)\right\}, & \text{if} \quad |\phi| = 0, 2\pi, 4\pi, \ldots \\ \dfrac{-2\pi}{5(\alpha_1 a)^3} \dfrac{\cos((\pi - |\phi|)\alpha_1 a)}{\sin(\pi\alpha_1 a)}, & \text{if} \quad |\phi| < 2\pi, \phi \neq 0, \end{cases} \quad \text{as } \alpha_1 a \to \infty. \tag{42}$$

Numerical checks have shown that this asymptotic result gives good agreement with numerical results for values of $\alpha_1 a \gtrsim 0{\cdot}75$ and excellent agreement when $\alpha_1 a \gtrsim 1$. However, when these expressions for the infinite sum are substituted into the asymptotic expression (30) for $A_{11}(\alpha, \phi)$ and checked against a numerical evaluation of equation (15) the results are disappointing. For a given value of ϕ graphs of A_{11} as a function of frequency exhibit a large number of peaks. The frequencies at which these peaks occur differs considerably between the numerical and asymptotic values, although the envelope of the magnitude shows good agreement. From the method described above it is clear that peaks occur when the real poles of the function $g(x)$ are equal to an integer. A small error in the pole location thus can have a large effect on the location of the peak, but a small error in the magnitude of the envelope function. The method may be repeated using a more accurate function for $g(x)$, for example from equation (28):

$$g(x) = \frac{|x| e^{ix|\phi|}}{[|x|\{(x^2 + \alpha^2 a^2)^2 - (\alpha_0 a)^4\} - (\alpha_1 a)^5]}. \tag{43}$$

If $x = \alpha_2 a$ is the positive real root of the quintic polynomial

$$x((x^2 + \alpha^2 a^2)^2 - (\alpha_0 a)^4) - (\alpha_1 a)^5 = 0, \tag{44}$$

it is clear that for heavy fluid-loading $\alpha_2 \approx \alpha_1$, and that $A_{11}(\alpha, \phi)$ may be approximated as

$$A_{11}(\alpha, \phi) \sim \begin{cases} -\dfrac{2\pi a}{5D\alpha_2^3}\left\{\cot\left(\dfrac{2\pi}{5}\right) + \cot(\pi\alpha_2 a)\right\}, & \text{if} \quad |\phi| = 0,\ 2\pi,\ 4\pi, \ldots, \\ -\dfrac{2\pi a}{5D\alpha_2^3} \dfrac{\cos((\pi - |\phi|)\alpha_2 a)}{\sin(\pi\alpha_2 a)}, & \text{if} \quad |\phi| < 2\pi, \phi \neq 0, \end{cases} \quad \text{as } \alpha_1 a \to \infty. \tag{45}$$

A simple interpretation of equation (45) is that the radial motion generated as a result of applying a radial line force to the cylindrical shell consists of disturbances which decay with distance from the application line, together with waves propagating away from the application line helically around the shell, whose wavenumbers in the tangential direction, $\pm \alpha_2$, are, in the heavy fluid-loading limit, the wavenumbers in the tangential direction of bending waves, propagating at angles $\tan^{-1}(\alpha_2/\alpha)$ to the axial direction, in an equivalent fluid-loaded plate. The heavy fluid-loading ensures that the decaying disturbance is only significant near to $\phi = 0$. This is reflected in the $\cot(2\pi/5)$ term in equation (45). The propagating waves, however, travel around the shell, and if an integer number of their wavelengths fit around the shell circumference reinforcement will occur leading to a standing wave pattern of growing magnitude. This reinforcement thus occurs when $\alpha_2 a$ is an integer, or equivalently, $\sin \pi\alpha_2 a = 0$. Thus peaks in A_{11} may be predicted at those frequencies for which $\sin \pi\alpha_2 a = 0$ at all values of ϕ except at the nodes of the standing wave pattern. At these resonance frequencies the nodes occur when $2|\phi|a$ is an odd number of

half-wavelengths, hence $|\phi|\alpha_2 a$ is an odd number of multiples of $\pi/2$, as is $(\pi - |\phi|)\alpha_2 a$, and nodes thus occur when $\cos((\pi - |\phi|)\alpha_2 a)$ is zero. From this it may be deduced that if ϕ is a rational multiple of π of the form $\phi = \pi l/m$, where l and m have no common factors and m is even, then in any frequency interval for which the receptance at 0 or π exhibits m peaks the receptance at ϕ will exhibit only $(m - 1)$ peaks. Thus, the formal analysis leading to equation (45) has produced analytic expressions for the receptance which are in agreement with a physical interpretation. In addition to predicting the frequencies of resonance, however, equation (45) also provides explicit expressions for the receptance at non-resonant frequencies. This can be important, for example, in predicting and understanding the peaks in the scattered sound field in line-constrained problems where the reaction force amplitudes depend on both frequency and geometry. That analysis is beyond the scope of this paper and will be reported separately.

The remaining elements of $\mathbf{A}(\alpha, \phi)$ will also be evaluated in the heavy fluid-loading limit. Thus,

$$A_{12}(\alpha, \phi) = \sum_{n=0}^{\infty} e_n S_{12}^{-1} \cos n\phi = - \sum_{n=0}^{\infty} e_n \frac{(S_{12}S_{33} - S_{13}S_{32})}{\Delta} \cos n\phi, \tag{46}$$

and replacing the summand by its large n form to obtain the leading order term in the heavy fluid-loading, $\alpha_1 a \to \infty$, asymptotic evaluation allows it to be written as

$$A_{12}(\alpha, \phi) \sim - \sum_{n=0}^{\infty} e_n S_{11}^{-1} \frac{(S_{12}S_{33} - S_{13}S_{32})}{(S_{22}S_{33} - S_{23}S_{32})} \cos n\phi, \tag{47}$$

where S_{11}^{-1} has already been approximated in two ways above. In the analysis which follows, for simplicity of exposition, it will be approximated using equation (29), but with the reservation that if the final result contains terms of the type $\cot(\alpha_1 a\pi)$, etc. then α_1 will be replaced by α_2, as if equation (28) had been used to approximate it. After some algebra it may be shown that the remaining factors in equation (47) may be expressed exactly, as

$$(S_{12}S_{33} - S_{13}S_{32}) = - E_1^2 \mathrm{i}\alpha(1 - \sigma)(n^2 - B^2)/2a^3, \tag{48}$$

$$(S_{22}S_{33} - S_{23}S_{32}) = E_1^2(1 - \sigma)(n^2 - P^2)(n^2 - Q^2)/2a^4, \tag{49}$$

where

$$P^2 = a^2(\rho_s \omega^2 h/E_1 - \alpha^2), \quad Q^2 = a^2(2\rho_s \omega^2 h/E_1(1 - \sigma) - \alpha^2), \tag{50, 51}$$

$$B^2 = - \sigma Q^2, \tag{52}$$

where these parameters are independent of both n and the fluid-loading parameter. Thus, using partial fractions,

$$\frac{(S_{12}S_{33} - S_{13}S_{32})}{(S_{22}S_{33} - S_{23}S_{32})} = \mathrm{i}\alpha a \left(\frac{X}{n^2 - Q^2} + \frac{Y}{n^2 - P^2} \right), \tag{53}$$

where

$$X = \frac{(Q^2 - B^2)}{(Q^2 - P^2)}, \quad Y = \frac{(-P^2 + B^2)}{(Q^2 - P^2)}, \tag{54, 55}$$

and hence the asymptotic form of $A_{12}(\alpha, \phi)$ for heavy fluid-loading is

$$A_{12}(\alpha, \phi) \sim \frac{\mathrm{i}\alpha a^5}{D} \sum_{n=0}^{\infty} \left(\frac{X}{(n^2 - Q^2)} + \frac{Y}{(n^2 - P^2)} \right) \frac{e_n n \cos n\phi}{(n^5 - (\alpha_1 a)^5)}. \tag{56}$$

Evaluating sums of this form in the heavy fluid-loading limit using, for example, the Poisson summation theorem described above, shows that

$$\sum_{n=0}^{\infty} \frac{e_n n \cos n\phi}{(n^2 - Q^2)(n^5 - (\alpha_1 a)^5)} \sim O\left(\frac{\ln(\alpha_1 a)}{(\alpha_1 a)^5}\right). \tag{57}$$

Thus,

$$A_{12}(\alpha, \phi) \sim O\left(\frac{\ln(\alpha_1 a)}{(\alpha_1 a)^5}\right) \quad \text{as } \alpha_1 a \to \infty. \tag{58}$$

Similarly, from equation (15)

$$A_{13}(\alpha, \phi) = -\sum_{n=0}^{\infty} e_n S_{13}^{-1} \sin n\phi = -\sum_{n=0}^{\infty} e_n \frac{(S_{12}S_{23} - S_{13}S_{22})}{\Delta} \sin n\phi. \tag{59}$$

Clearly, this is identically zero when $|\phi| = 0, 2\pi, 4\pi, \ldots$. For other values of ϕ the asymptotic heavy fluid-loading approximation is obtained as before:

$$A_{13}(\alpha, \phi) \sim -\sum_{n=0}^{\infty} e_n S_{11}^{-1} \frac{(S_{12}S_{23} - S_{13}S_{22})}{(S_{22}S_{33} - S_{23}S_{32})} \sin n\phi, \tag{60}$$

and, for large n,

$$\frac{(S_{12}S_{23} - S_{13}S_{22})}{(S_{22}S_{33} - S_{23}S_{32})} \sim -\frac{1}{n}, \quad \text{as } n \to \infty. \tag{61}$$

Thus,

$$A_{13}(\alpha, \phi) \sim \frac{a^4}{D} \sum_{n=0}^{\infty} \frac{e_n \sin n\phi}{n^5 - (\alpha_1 a)^5} = \frac{a^4 \operatorname{sign}(\phi)}{\mathrm{i}D} \sum_{n=-\infty}^{\infty}{}' \frac{n e^{\mathrm{i}n|\phi|}}{|n|(|n|^5 - (\alpha_1 a)^5)}$$

$$= \frac{a^4 \operatorname{sign}(\phi)}{\mathrm{i}D} \sum_{m=-\infty}^{\infty} g(m), \tag{62}$$

in which the $'$ on the summation indicates that $n = 0$ is omitted, and where

$$g(x) = \frac{f(x) \mathrm{e}^{\mathrm{i}x|\phi|}}{(|x|^5 - (\alpha_1 a)^5)}, \tag{63}$$

with $f(x)$ any suitable, continuous function chosen to ensure that $g(x)$ satisfies the requirements of the Poisson summation theorem, for example,

$$f_N(x) = \begin{cases} 1 & \text{for} \quad x \geqslant 1/N, \\ Nx & \text{for} \quad |x| \leqslant 1/N, \\ -1 & \text{for} \quad x \leqslant -1/N. \end{cases} \tag{64}$$

Thus, when N is large

$$G(s) = \int_0^{\infty} \frac{(\mathrm{e}^{-\mathrm{i}(s-|\phi|)x} - \mathrm{e}^{\mathrm{i}(s-|\phi|)x})}{x^5 - (\alpha_1 a)^5} \mathrm{d}x, \tag{65}$$

and clearly

$$G(|\phi|) = 0. \tag{66}$$

For $s \neq |\phi|$, using contour integration to close the integration contour in either the upper or lower halves of the complex plane, as before, the heavy fluid-loading form of G is found to be

$$G(s) \sim -\frac{2\pi i}{5(\alpha_1 a)^4}\text{sign}(s-|\phi|)e^{i|s-|\phi||\alpha_1 a} \quad \text{as } \alpha_1 a \to \infty, \quad s \neq |\phi|. \tag{67}$$

Thus, after evaluating another geometric series and simplifying the resulting expressions

$$\sum_{m=-\infty}^{\infty} g(m) \sim -\frac{2\pi i}{5(\alpha_1 a)^4}\frac{\sin((|\phi|-\pi)\alpha_1 a)}{\sin(\pi\alpha_1 a)}. \tag{68}$$

Noting again that the pole location is better approximated by $\alpha_2 a$ where this is the root of equation (44), the heavy fluid-loading asymptotic approximation to $A_{13}(\alpha, \phi)$ is obtained as

$$A_{13}(\alpha, \phi)\begin{cases} \equiv 0, & \text{if } |\phi| = 0,\ 2\pi,\ 4\pi, \ldots, \\ \sim \dfrac{2\pi}{5D\alpha_2^4}\,\text{sign}(\phi)\dfrac{\sin((\pi-|\phi|)\alpha_2 a)}{\sin(\pi\alpha_2 a)}, & \text{if } |\phi| < 2\pi,\ \phi \neq 0, \end{cases} \quad \text{as } \alpha_1 a \to \infty. \tag{69}$$

This may be interpreted as the leading order radial motion generated as a result of applying a line force in the tangential direction consists of waves propagating helically away from the line force, again with tangential wavenumbers $\pm\alpha_2$, the wavenumber in the tangential direction of bending waves in an equivalent fluid-loaded plate, which again form a standing wave pattern if an integer number of wavelengths fit around the circumference. Hence the possible peaks in a graph of A_{13} may be predicted to occur at the same frequencies as those of A_{11}. In the radial force case the disturbance is an even function of ϕ, but with a tangential force it is an odd function of ϕ. Hence $\phi = 0$ and π are nodes of the standing wave pattern. If ϕ is any rational multiple of π, $\phi = \pi l/m$, where l and m have no common factors, then nodes of the standing wave pattern occur at ϕ for one of each m possible successive resonance frequencies, and hence the corresponding peaks will be omitted from a graph of A_{13} as a function of frequency. By comparing equations (45) and (69) it may be seen that the magnitude of A_{13} is smaller than that of A_{11} by a factor which is of order $1/\alpha_2 a$ in the heavy fluid-loading limit.

From equation (15)

$$A_{21}(\alpha, \phi) = \sum_{n=0}^{\infty} e_n S_{21}^{-1}\cos n\phi = -\sum_{n=0}^{\infty} e_n S_{12}^{-1}\cos n\phi = -A_{12}(\alpha, \phi). \tag{70}$$

Hence,

$$A_{21}(\alpha, \phi) \sim O\left(\frac{\ln(\alpha_1 a)}{(\alpha_1 a)^5}\right) \quad \text{as } \alpha_1 a \to \infty. \tag{71}$$

Similarly,

$$A_{22}(\alpha, \phi) = \sum_{n=0}^{\infty} e_n S_{22}^{-1}\cos n\phi. \tag{72}$$

The (2, 2) element of the inverse matrix of $\mathbf{S}$ may be written

$$\begin{aligned} S_{22}^{-1} &= (S_{11}S_{33} - S_{13}S_{31})/\Delta \\ &= \frac{S_{33}}{(S_{22}S_{33} - S_{23}S_{32})} \\ &\quad + \frac{1}{\Delta}\left\{\frac{S_{33}S_{12}(S_{21}S_{33} - S_{23}S_{31}) - S_{33}S_{13}(S_{21}S_{32} - S_{22}S_{31})}{(S_{22}S_{33} - S_{23}S_{32})} - S_{13}S_{31}\right\}, \end{aligned} \tag{73}$$

using the definition of Δ given by equation (24), where the first term is independent of the fluid-loading parameter, and the second term is $O(1/(\alpha_1 a)^5)$ and is of the type noted previously. For large values of n, using equations (12) the second term may be approximated as

$$\frac{1}{\Delta}\{\cdots\} \sim \frac{S_{11}^{-1}}{n^4} \quad \text{as } n \to \infty. \tag{74}$$

Applying the method described previously to this component of $A_{22}(\alpha, \phi)$ would, therefore, give pole contributions of higher order in $1/\rho$ than those already neglected in forming the approximation. Thus, only the $O(1)$, first term of equation (73) needs to be evaluated to find the leading order asymptotic approximation to $A_{22}(\alpha, \phi)$. An expression for $(S_{22}S_{33} - S_{23}S_{32})$ is given by equation (49). In terms of Q, S_{33}, given by equation (12i) may be written

$$S_{33} = E_1(n^2 - (1 - \sigma)Q^2/2)/a^2. \tag{75}$$

Thus,

$$A_{22}(\alpha, \phi) \sim \frac{2a^2}{E_1(1 - \sigma)}\left\{\sum_{n=0}^{\infty} \frac{e_n(n^2 - (1 - \sigma)Q^2/2)\cos n\phi}{(n^2 - Q^2)(n^2 - P^2)} + O\left(\frac{1}{(\alpha_1 a)^5}\right)\right\}. \tag{76}$$

These terms may not be replaced by their form for large values of n, but may be expressed in terms of partial fractions as

$$A_{22}(\alpha, \phi) \sim \frac{1/(1 + \sigma)}{\rho_s \omega^2 h}\left\{\sum_{n=0}^{\infty} e_n \left\{\frac{Q^2(1 + \sigma)}{(n^2 - Q^2)} - \frac{2P^2 - (1 - \sigma)Q^2}{(n^2 - P^2)}\right\}\cos n\phi + O\left(\frac{1}{(\alpha_1 a)^5}\right)\right\}, \tag{77}$$

where sums of this form are given in, for example reference [25, p. 40], or may be evaluated using the Poisson summation theorem method, as

$$\sum_{n=0}^{\infty} \frac{e_n \cos n\phi}{(n^2 - Q^2)} = -\frac{\pi \cos[Q((2m + 1)\pi - |\phi|)]}{Q \sin Q\pi}, \quad 2m\pi \leqslant |\phi| \leqslant (2m + 2)\pi. \tag{78}$$

By setting $m = 0$ in equation (78) the relevant range $|\phi| \leqslant 2\pi$ is obtained. However, as noted after equation (42), in order for the peak frequencies to agree with those obtained numerically the poles must be located fairly accurately. The poles of S_{22}^{-1} do not in general occur at exactly P and Q, but at the zeros of Δ near to P and Q, P_2 and Q_2 say, which differ from P and Q by an $O(1/\rho)$ correction and which may be approximated for heavy fluid-loading as

$$P_2 \sim P - F(\alpha, P)/2PE_1^2(1 - \sigma)(P^2 - Q^2)S_{11}(\alpha, P), \tag{79}$$

$$Q_2 \sim Q + F(\alpha, Q)/2QE_1^2(1 - \sigma)(P^2 - Q^2)S_{11}(\alpha, Q), \tag{80}$$

where

$$F(\alpha, n) = S_{13}(S_{21}S_{32} - S_{22}S_{33}) - S_{12}(S_{21}S_{33} - S_{23}S_{31}), \tag{81}$$

and in which $\mathrm{H}_\nu'(\gamma a)/\mathrm{H}_\nu(\gamma a)$ may be further approximated if required as

$$\mathrm{H}_\nu'(\gamma a)/\mathrm{H}_\nu(\gamma a) \sim \begin{cases} \mathrm{i} - 1/2\gamma a & \nu \ll \gamma a, \\ -\nu\{1 - \mathrm{i}(e\gamma a/2\nu)^{2\nu}\}/\gamma a & \nu \gg \gamma a. \end{cases} \tag{82}$$

Using equation (78), and noting the more accurate values for the pole locations, P_2 and Q_2, the leading order asymptotic approximation for $A_{22}(\alpha, \phi)$ is thus

$$A_{22}(\alpha, \phi) \sim \frac{\pi/(1+\sigma)}{\rho_s \omega^2 h}\left\{\frac{(2P^2-(1-\sigma)Q^2)}{P}\frac{\cos P_2(\pi-|\phi|)}{\sin \pi P_2} - Q(1+\sigma)\frac{\cos Q_2(\pi-|\phi|)}{\sin \pi Q_2}\right\},$$

$$|\phi| \leqslant 2\pi \quad \text{as } \alpha_1 a \to \infty, \tag{83}$$

where P and Q are given in equations (50, 51) and P_2 and Q_2 by equations (79–82). Each of the terms making up A_{22} in equation (83) has the same form as those in equation (45), but with the tangential wavenumbers given by $\pm P_2$ and $\pm Q_2$, respectively, which are independent of the fluid density, as are their amplitudes, and may thus be interpreted in a similar way to equation (45) but with the appropriate wavenumbers. It should be noted here that depending on the size of α either P_2 or both P_2 and Q_2 *may* be imaginary. If either of them is imaginary then the shell displacement corresponding to that wavenumber simply decays with distance from the application line and hence cannot lead to resonant behaviour, or peaks in the graph of A_{22} as a function of frequency. It may be noted here that when $\alpha = 0$ equation (83) reduces to the exact result

$$A_{22}(0, \phi) \equiv -\frac{\pi Q \cos Q(\pi-|\phi|)}{\rho_s \omega^2 h \sin \pi Q}. \tag{84}$$

The element $A_{23}(\alpha, \phi)$ is

$$A_{23}(\alpha,\phi) = -\sum_{n=0}^{\infty} e_n S_{23}^{-1} \sin n\phi = \sum_{n=0}^{\infty} e_n \frac{(S_{11}S_{23} - S_{13}S_{21})}{\Delta} \sin n\phi. \tag{85}$$

Clearly, this is identically zero when $|\phi| = 0, 2\pi, 4\pi, \ldots$. For other values of ϕ the summand is manipulated as follows:

$$\frac{(S_{11}S_{23} - S_{13}S_{21})}{\Delta} = \frac{S_{23}}{(S_{22}S_{33} - S_{23}S_{32})}$$

$$+ \frac{1}{\Delta}\left\{\frac{S_{23}S_{12}(S_{21}S_{33} - S_{23}S_{31}) - S_{23}S_{13}(S_{21}S_{32} - S_{22}S_{31})}{(S_{22}S_{33} - S_{23}S_{32})} - S_{13}S_{21}\right\}. \tag{86}$$

The first term of this is again independent of the fluid-loading parameter, and the second term is $O(1/(\alpha_1 a)^5)$ and is of the type noted previously. For large values of n, using equations (12) the second term may be approximated as

$$\frac{1}{\Delta}\{\cdots\} \sim \frac{S_{11}^{-1}}{n^3} \quad \text{as } n \to \infty, \tag{87}$$

which ensures that any pole contributions to the Poisson summation evaluation of the sum of the second term would be proportional to $O(1/(\alpha_1 a)^6)$ terms and thus of higher order than the $O(1/(\alpha_1 a)^5)$ terms already neglected in making the approximation. Thus, only the first, $O(1)$ term of equation (86) needs to be summed in order to find the leading order asymptotic approximation to $A_{23}(\alpha, \phi)$ for heavy fluid-loading. Hence, making use of equations (12f) and (49), $A_{23}(\alpha, \phi)$ may be written as

$$A_{23}(\alpha, \phi) = -\operatorname{sign}(\phi)\frac{i\alpha(1+\sigma)a^3}{E_1(1-\sigma)}\left\{\sum_{n=0}^{\infty}\frac{e_n n \sin n|\phi|}{(n^2-Q^2)(n^2-P^2)} + O\left(\frac{1}{(\alpha_1 a)^5}\right)\right\}. \tag{88}$$

This infinite summation may be evaluated by noting that

$$\sum_{n=0}^{\infty} \frac{e_n n \sin n|\phi|}{(n^2 - Q^2)(n^2 - P^2)} = \frac{1}{P^2 - Q^2} \sum_{n=0}^{\infty} \left\{ \frac{1}{(n^2 - P^2)} - \frac{1}{(n^2 - Q^2)} \right\} \mathrm{e}_n n \sin n|\phi|$$

$$= \frac{1}{Q^2 - P^2} \frac{\mathrm{d}}{\mathrm{d}|\phi|} \sum_{n=0}^{\infty} \left\{ \frac{1}{(n^2 - P^2)} - \frac{1}{(n^2 - Q^2)} \right\} \mathrm{e}_n \cos n|\phi|, \quad (89)$$

and that the method for summations of this type was used to calculate A_{22}. Thus, noting again that the pole locations are more accurately described as P_2 and Q_2,

$$A_{23}(\alpha, \phi) \begin{cases} \equiv 0, & \text{if } |\phi| = 0,\ 2\pi, \ldots \\ \sim \dfrac{\mathrm{i}\alpha a \pi \operatorname{sign}(\phi)}{\rho_s \omega^2 h} \left\{ \dfrac{\sin P_2(\pi - |\phi|)}{\sin P_2 \pi} - \dfrac{\sin Q_2(\pi - |\phi|)}{\sin Q_2 \pi} \right\}, & \text{if } |\phi| < 2\pi,\ \phi \neq 0, \\ & \text{as } \alpha_1 a \to \infty. \end{cases} \quad (90)$$

Each of the terms making up A_{23} in equation (90) has the same form as those in equation (69), but with tangential wavenumbers given by $\pm P_2$ and $\pm Q_2$, respectively, and may be interpreted in a similar way to equation (69), but using the appropriate wavenumbers.

From equation (15)

$$A_{31}(\alpha, \phi) = \sum_{n=0}^{\infty} e_n S_{31}^{-1} \sin n\phi = \sum_{n=0}^{\infty} e_n S_{13}^{-1} \sin n\phi = -A_{13}(\alpha, \phi). \quad (91)$$

Hence,

$$A_{31}(\alpha, \phi) \begin{cases} \equiv 0, & \text{if } |\phi| = 0,\ 2\pi,\ 4\pi, \ldots, \\ \sim -\dfrac{2\pi}{5D\alpha_2^4} \operatorname{sign}(\phi) \dfrac{\sin((\pi - |\phi|)\alpha_2 a)}{\sin(\pi \alpha_2 a)}, & \text{if } |\phi| < 2\pi,\ \phi \neq 0, \end{cases} \quad \text{as } \alpha_1 a \to \infty. \quad (92)$$

Similarly,

$$A_{32}(\alpha, \phi) = \sum_{n=0}^{\infty} e_n S_{32}^{-1} \sin n\phi = -\sum_{n=0}^{\infty} e_n S_{23}^{-1} \sin n\phi = A_{23}(\alpha, \phi). \quad (93)$$

Hence,

$$A_{32}(\alpha, \phi) \begin{cases} \equiv 0, & \text{if } |\phi| = 0,\ 2\pi, \ldots \\ \sim \dfrac{\mathrm{i}\alpha a \pi \operatorname{sign}(\phi)}{\rho_s \omega^2 h} \left\{ \dfrac{\sin P_2(\pi - |\phi|)}{\sin P_2 \pi} - \dfrac{\sin Q_2(\pi - |\phi|)}{\sin Q_2 \pi} \right\}, & \text{if } |\phi| < 2\pi,\ \phi \neq 0, \\ & \text{as } \alpha_1 a \to \infty. \end{cases} \quad (94)$$

The remaining element $A_{33}(\alpha, \phi)$ is evaluated in a similar way to $A_{22}(\alpha, \phi)$. Hence, from equation (15)

$$A_{33}(\alpha, \phi) = \sum_{n=0}^{\infty} e_n S_{33}^{-1} \cos n\phi, \quad (95)$$

where

$$S_{33}^{-1} = (S_{11} S_{22} - S_{12} S_{21})/\Delta$$

$$= \frac{S_{22}}{(S_{22} S_{33} - S_{23} S_{32})} + \frac{1}{\Delta} \left\{ \frac{S_{12} S_{23}(S_{21} S_{32} - S_{31} S_{22}) - S_{22} S_{13}(S_{21} S_{32} - S_{22} S_{31})}{(S_{22} S_{33} - S_{23} S_{32})} \right\}, \quad (96)$$

in which the second term, which is $O(1/(\alpha_1 a)^5)$, may be approximated for large values of n, as

$$\frac{1}{\Delta}\{\cdots\} \sim \frac{S_{11}^{-1}}{n^2} \quad \text{as } n \to \infty, \tag{97}$$

which is sufficient to ensure that any pole contributions to the Poisson summation evaluation of the sum of the second term of equation (96) would be proportional to $O(1/(\alpha_1 a)^5)$ terms and thus of the same order as those already neglected in making the heavy fluid-loading approximation. Thus, again only the $O(1)$ first term of equation (96) needs to be used in equation (95) to find the leading order term of $A_{33}(\alpha, \phi)$. Writing, from equation (12e),

$$S_{22} = E_1(1 - \sigma)(n^2 - R^2)/2a^2, \tag{98}$$

where

$$R^2 = a^2(2\rho_s\omega^2 h/E_1 - 2\alpha^2)/(1 - \sigma), \tag{99}$$

allows the leading order term of $A_{33}(\alpha, \phi)$ to be expressed as

$$A_{33}(\alpha, \phi) \sim \frac{a^2}{E_1}\left\{\sum_{n=0}^{\infty} \frac{e_n(n^2 - R^2)\cos n|\phi|}{(n^2 - Q^2)(n^2 - P^2)} + O\left(\frac{1}{(\alpha_1 a)^5}\right)\right\}$$

$$\sim \frac{1}{\rho_s\omega^2 h}\frac{1 - \sigma}{1 + \sigma}\left\{\sum_{n=0}^{\infty} e_n\left\{\frac{Q^2 - R^2}{n^2 - Q^2} + \frac{R^2 - P^2}{n^2 - P^2}\right\}\cos n|\phi| + O\left(\frac{1}{(\alpha_1 a)^5}\right)\right\}. \tag{100}$$

These are sums which have been evaluated in equation (78). Thus, noting again the corrected pole locations P_2 and Q_2,

$$A_{33}(\alpha, \phi) \sim \frac{\pi}{\rho_s\omega^2 h}\frac{1 - \sigma}{1 + \sigma}\left\{\frac{(R^2 - Q^2)\cos Q_2(\pi - |\phi|)}{Q \sin \pi Q_2} + \frac{(P^2 - R^2)\cos P_2(\pi - |\phi|)}{P \sin \pi P_2}\right\},$$

$$|\phi| \leqslant 2\pi \quad \text{as } \alpha_1 a \to \infty, \tag{101}$$

where P and Q are given in equations (50, 51), P_2 and Q_2 by equations (79–82), and R is given by equation (99). The structure of equation (101) is similar to that of equation (83) and may be interpreted in a similar way. Thus equations (45), (58), (69), (71), (83), (90), (92), (94) and (101) provide heavy fluid-loading asymptotic approximations to all the elements of $\mathbf{A}(\alpha, \phi)$, and show explicitly the dependence of these quantities on the parameters of the problem.

4. NUMERICAL RESULTS

The leading order asymptotic results for heavy fluid-loading, derived in section 3, have been evaluated numerically, for a steel cylindrical shell, for which the values $E = 19{\cdot}5 \times 10^{10}$, $\rho_s = 7700$, $\sigma = 0{\cdot}29$ have been used, of radius 5 m and thickness 0·05 m, surrounded by water, $\rho = 1000$, $c = 1500$. A small amount of damping has been included in the calculations by including the complex factors $(1 - i\eta_s)$ and $(1 - i\eta)$ in E and c, respectively, where $\eta = \eta_s = 0{\cdot}001$. It should be noted that in the absence of damping, and unless P_2 or Q_2 is imaginary, the asymptotic results for the receptance are either purely real or purely imaginary, with infinite values possible at the peak frequencies. The introduction of a small amount of damping introduces a correspondingly small imaginary or real part, respectively, to the receptance and ensures that whilst the peak values are large they are finite, with that value determined by the amount of damping. The numerical results confirm

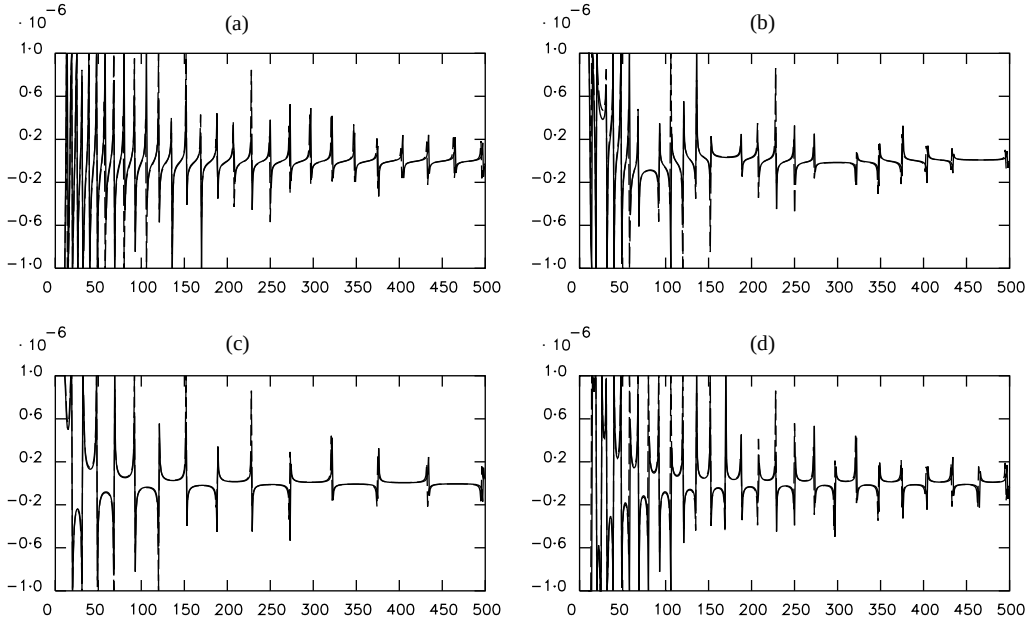

Figure 1. $\mathrm{Re}\{A_{11}(\alpha, \phi)\}$ for steel shell, $a = 5$, $h = 0{\cdot}05$, in water, as a function of frequency (Hz). $\alpha = k\cos\theta$, $\theta = 45°$: (a) $\phi = 0°$; (b) $\phi = 30°$; (c) $\phi = 90°$; (d) $\phi = 180°$: ——, asymptotic result (45); – – –, numerical summation.

this, but as the small imaginary or real part due to the damping adds little extra to the comparison of the asymptotic and numerical results they are omitted here for reasons of space unless the real and imaginary parts are of comparable magnitude. The real and/or imaginary parts are presented here rather than, for example, the modulus because the sign (or phase) of the receptance is important in problems with line constraints. The asymptotic results are compared with results obtained from a numerical summation of the first 1000 terms of equation (15). In the results presented here α, the axial wavenumber, is proportional to the excitation frequency, $\alpha = k\cos\theta$, and the graphs are all functions of frequency $f = \omega/2\pi$. The maximum frequency shown in each plot is 500 Hz, corresponding to $ka \approx 10{\cdot}5$, and chosen to illustrate the range of applicability of the asymptotic results. The asymptotic results are shown as a solid line and the numerical summation as a broken line.

Figure 1 shows the results of plotting the real part of $A_{11}(\alpha, \phi)$ for $\theta = 45°$, and $\phi = 0$, 30, 90 and 180°. As discussed after equation (45), the frequencies at which peaks occur coincide for $\phi = 0$ and 180°. At $\phi = 30°$, $(\pi/6)$, every sixth peak is missing, and at $\phi = 90°$, $(\pi/2)$, every second peak is missing compared to those at $\phi = 0$ and 180°. Over most of the frequency range shown, the asymptotic and numerical results are indistinguishable. At the higher frequencies there are very slight discrepancies in the frequencies at which peaks occur, which presumably could be reduced if required by including extra terms in equations (43) and (44) to obtain a more accurate value for α_2. Further results, not presented here, show that the accuracy of the asymptotic result remains very good when the frequency is increased to more than 1000 Hz, even though the assumptions of heavy fluid-loading, inequalities (19, 20), are not satisfied then. Corresponding plots of the imaginary part of A_{11}, on the same scale also show excellent agreement between the asymptotic and numerical results and indicate that it is approximately zero except near the peaks in the real part, and are omitted here.

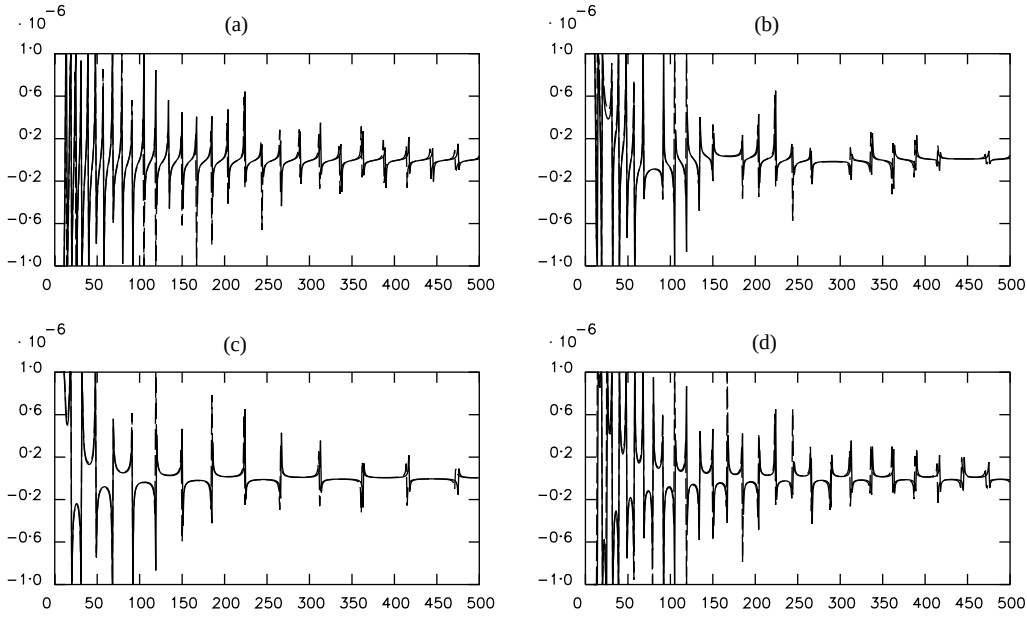

Figure 2. $\mathrm{Re}\{A_{11}(\alpha, \phi)\}$ for steel shell, $a = 5$, $h = 0{\cdot}05$, in water, as a function of frequency (Hz). $\alpha = k\cos\theta$, $\theta = 90°$: (a) $\phi = 0°$; (b) $\phi = 30°$; (c) $\phi = 90°$; (d) $\phi = 180°$: ——, asymptotic result (45); – – –, numerical summation.

Figure 2 shows the results of plotting the real part of $A_{11}(\alpha,\phi)$ for $\theta = 90°$ and $\phi = 0$, 30, 90 and 180°. Again, the imaginary part on the same scale is approximately zero except near the peaks in the real part, and is omitted here. There is again excellent agreement between the asymptotic and numerical results. The frequencies at which peaks occur differ from those obtained when $\theta = 45°$, but the frequencies for peaks when $\phi = 0°$ again coincide with those for $\phi = 180°$, whilst for $\phi = 30°$ every sixth peak is missing and for $\phi = 90°$ every second peak is missing.

Figure 3 shows the results of plotting the real part of $A_{13}(\alpha, \phi)$ for $\theta = 45°$, $\phi = 30$ and 90°, and $\theta = 90°$, $\phi = 30$ and 90°. Clearly, if $\phi = 0$ or 180° $A_{13}(\alpha,\phi)$ is identically zero. There is good agreement between the asymptotic and numerical results, although the curves can be distinguished at the lower frequencies shown. As predicted, the frequency of each of the peaks shown in Figures 3(a) and 3(b) is also the frequency of a peak in Figures 1(a) and 1(d). Compared to Figures 1(a) and 1(d), Figure 3(a) has every sixth peak missing, and Figure 3(b) has every second peak missing. As predicted, however, these are not the same missing peaks as those of Figures 1(b) and 1(c). Similarly, the frequency of each of the peaks shown in Figures 3(c) and 3(d) is also the frequency of a peak in Figures 2(a) and 2(d), and compared to Figures 2(a) and 2(d) Figure 3(c) has every sixth peak missing and Figure 3(d) has every second peak missing. These are also not the same missing peaks as those in Figures 2(b) and 2(c).

Figure 4 shows the real part of $A_{22}(\alpha, \phi)$ for $\theta = 45°$, $\phi = 0$, 30, 90 and 180°. The numerical and asymptotic results exhibit excellent agreement. These plots differ from the previous plots because the level is much lower, and there are no sharp peaks. The level just decreases as the frequency is increased. This is because the value of P calculated from equation (50) is imaginary if $\cos\theta > c\sqrt{\rho_s/E(1-\sigma^2)}$, which for a steel shell in water is equivalent to $\theta < 71{\cdot}85°$, and Q calculated from equation (51) is imaginary if $\cos\theta > c\sqrt{2\rho_s/E(1-\sigma^2)(1-\sigma)}$, which for a steel shell in water is equivalent to $\theta < 58{\cdot}49°$.

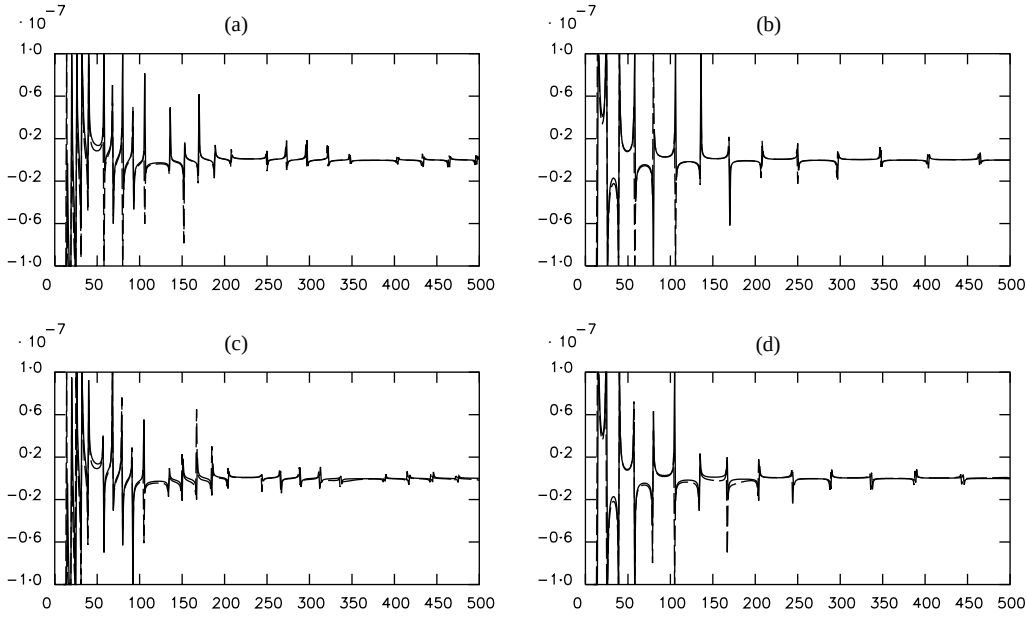

Figure 3. $\mathrm{Re}\{A_{13}(\alpha, \phi)\}$ for steel shell, $a = 5$, $h = 0{\cdot}05$, in water, as a function of frequency (Hz). $\alpha = k\cos\theta$: (a) $\theta = 45^\circ$, $\phi = 30^\circ$; (b) $\theta = 45^\circ$, $\phi = 90^\circ$; (c) $\theta = 90^\circ$, $\phi = 30^\circ$; (d) $\theta = 90^\circ$, $\phi = 90^\circ$: ——, asymptotic result (69); numerical summation.

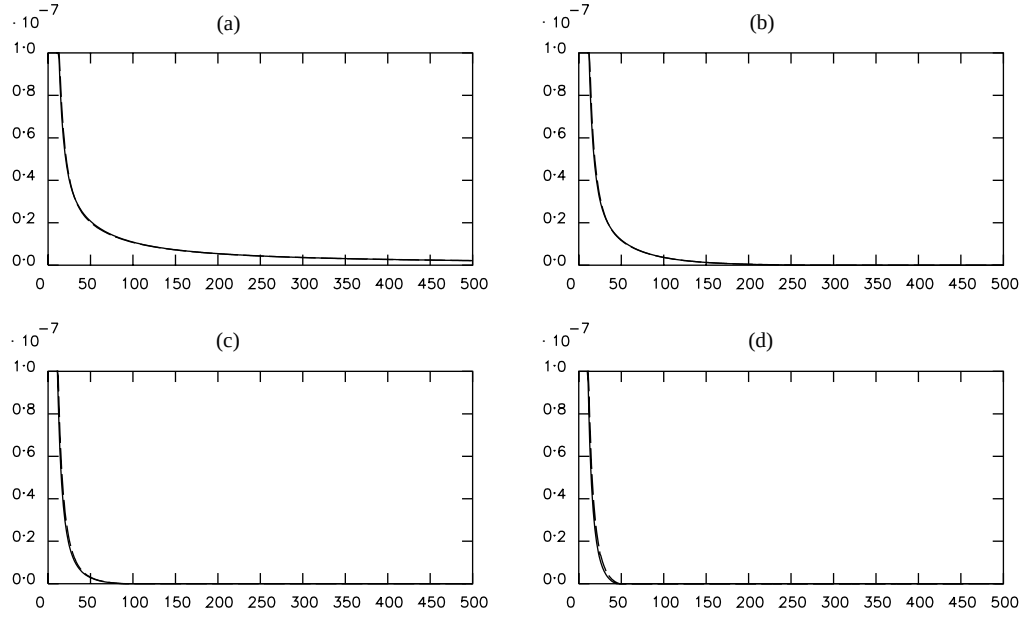

Figure 4. $\mathrm{Re}\{A_{22}(\alpha, \phi)\}$ for steel shell, $a = 5$, $h = 0.05$, in water, as a function of frequency (Hz). $\alpha = k\cos\theta$, $\theta = 45^\circ$: (a) $\phi = 0^\circ$; (b) $\phi = 30^\circ$; (c) $\phi = 90^\circ$; (d) $\phi = 180^\circ$: ——, asymptotic result (83); – – –, numerical summation.

Thus, for $\theta = 45^\circ$, both P and Q are approximately imaginary and no sharp peaks are expected. Figure 5 shows the real part of $A_{22}(\alpha, \phi)$ for $\theta = 90^\circ$, $\phi = 0$, 30, 90 and 180°. The numerical and asymptotic results are identical, as noted in equation (84). These plots differ

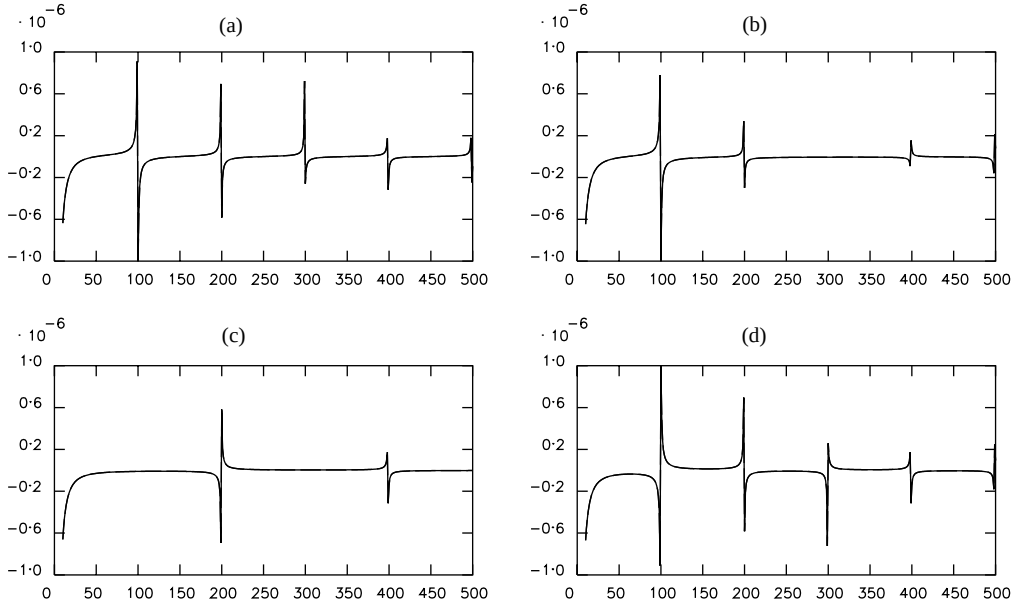

Figure 5. $\mathrm{Re}\{A_{22}(\alpha, \phi)\}$ for steel shell, $a = 5$, $h = 0{\cdot}05$, in water, as a function of frequency (Hz). $\alpha = k\cos\theta$, $\theta = 90°$: (a) $\phi = 0°$; (b) $\phi = 30°$; (c) $\phi = 90°$; (d) $\phi = 180°$: ——, asymptotic result (83); numerical summation.

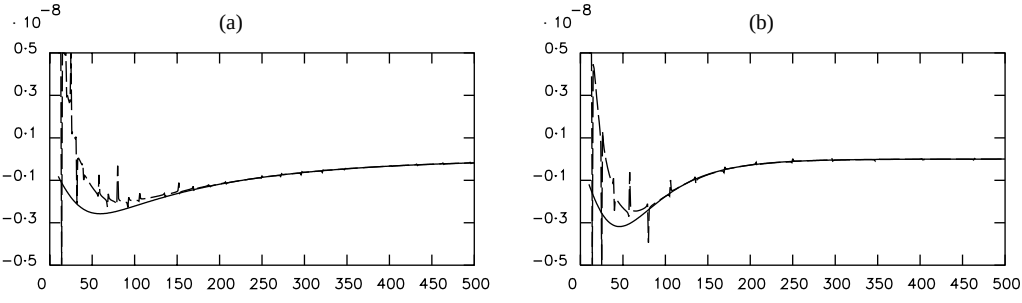

Figure 6. $\mathrm{Im}\{A_{23}(\alpha, \phi)\}$ for steel shell, $a = 5$, $h = 0{\cdot}05$, in water, as a function of frequency (Hz). $\alpha = k\cos\theta$, $\theta = 45°$: (a) $\phi = 30°$; (b) $\phi = 90°$: ——, asymptotic result (90); numerical summation.

considerably in character from those of Figure 4. When $\theta = 90°$, both P and Q are approximately real and hence sharp peaks occur in the plots at frequencies for which Q is approximately an integer. Again, it is evident from these figures that for $\phi = 0$ and $180°$ the frequencies of the peaks are identical. For $\phi = 90°$ every second peak is missing, and although the frequency range plotted in Figure 5(b) is not large enough to show this for $\phi = 30°$ every sixth peak is missing. Since there are far fewer peaks in Figure 5 than in Figure 2 the tangential wavenumber for motion of the shell which is predominantly longitudinal is much less than the tangential wavenumber for predominantly bending motion in this steel shell.

Figure 6 shows the imaginary part of $A_{23}(\alpha, \phi)$ for $\theta = 45°$, $\phi = 30$ and $90°$. $A_{23}(\alpha, \phi)$ is identically zero when $\phi = 0$ or $180°$. At frequencies above approximately 100 Hz the asymptotic and numerical results show good agreement. The asymptotic result exhibits no

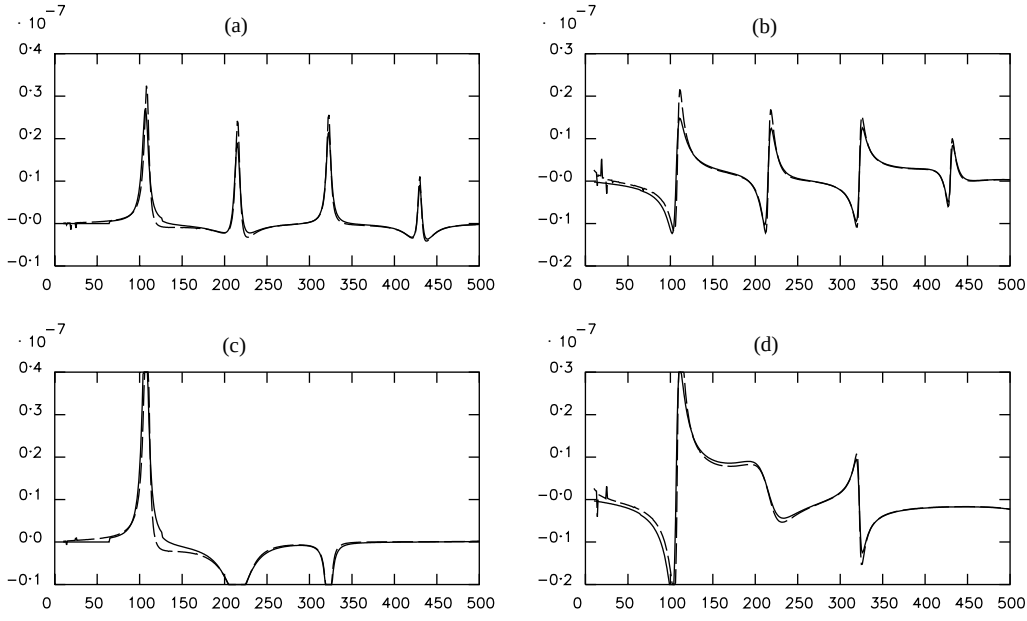

Figure 7. $A_{23}(\alpha, \phi)$ for steel shell, $a = 5$, $h = 0.05$, in water, as a function of frequency (Hz). $\alpha = k \cos\theta$, $\theta = 80°$: (a) $\mathrm{Re}\{A_{23}\}$, $\phi = 30°$; (b) $\mathrm{Im}\{A_{23}\}$, $\phi = 30°$; (c) $\mathrm{Re}\{A_{23}\}$, $\phi = 90°$; (d) $\mathrm{Im}\{A_{23}\}$, $\phi = 90°$: ——, asymptotic result (90); ——, numerical summation.

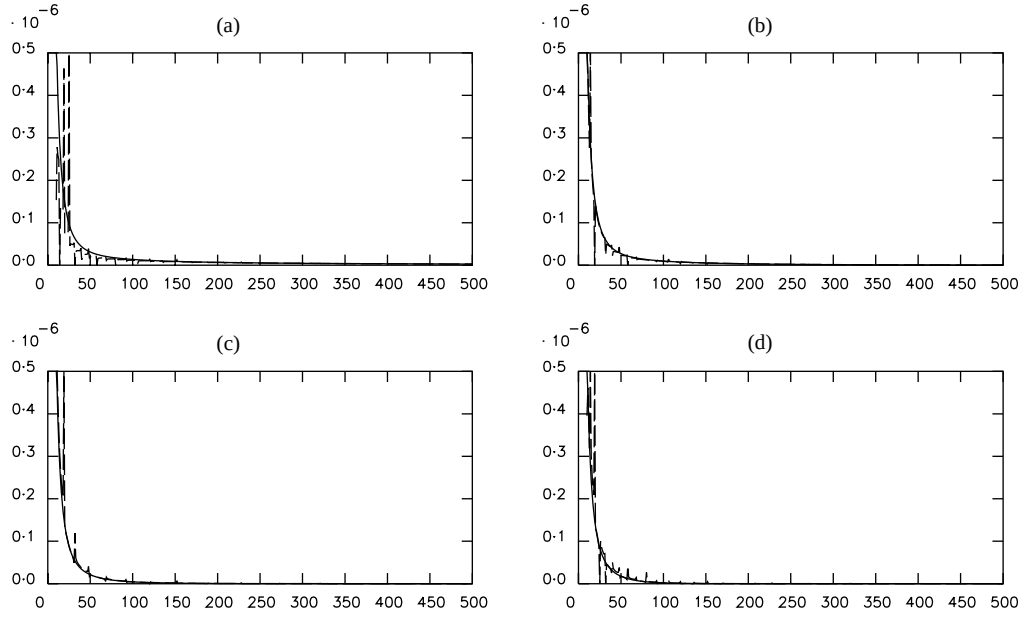

Figure 8. $\mathrm{Re}\{A_{33}(\alpha, \phi)\}$ for steel shell, $a = 5$, $h = 0{\cdot}05$, in water, as a function of frequency (Hz): $\alpha = k \cos\theta$, $\theta = 45°$; (a) $\phi = 0°$; (b) $\phi = 30°$; (c) $\phi = 90°$; (d) $\phi = 180°$: ——, asymptotic result (101); – – –, numerical summation.

sharp peaks because $\theta = 45°$ is in the range where P and Q are imaginary. At frequencies below approximately 100 Hz the numerical result differs from the asymptotic result and also exhibits sharp peaks. The levels of the asymptotic results are low, compared even to

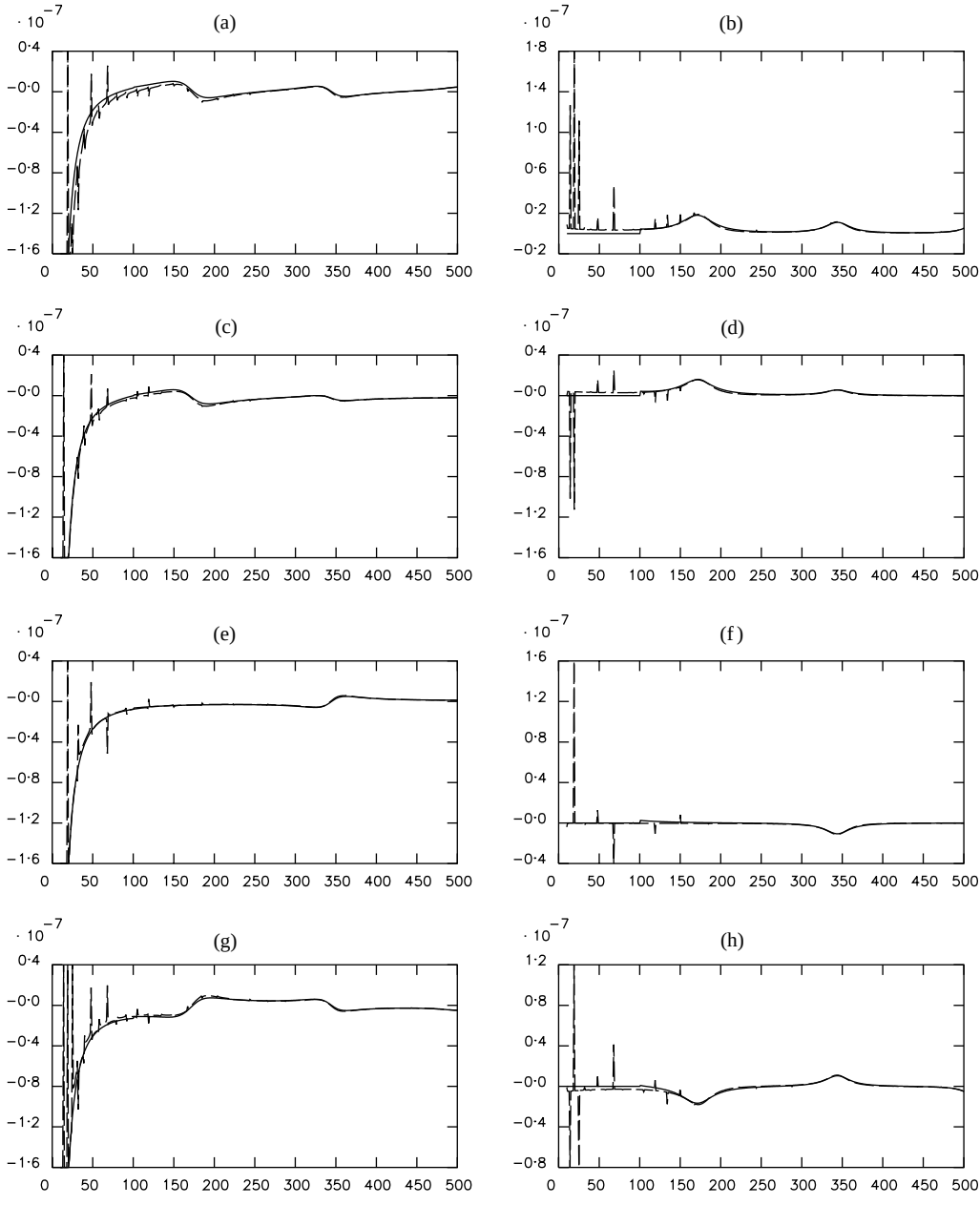

Figure 9. $A_{33}(\alpha, \phi)\}$ for steel shell, $a = 5$, $h = 0{\cdot}05$, in water, as a function of frequency (Hz). $\alpha = k \cos\theta$, $\theta = 90°$: (a) $\mathrm{Re}\{A_{33}\}$, $\phi = 0°$; (b) $\mathrm{Im}\{A_{33}\}$, $\phi = 0°$; (c) $\mathrm{Re}\{A_{33}\}$, $\phi = 30°$; (d) $\mathrm{Im}\{A_{33}\}$, $\phi = 30°$; (e) $\mathrm{Re}\{A_{33}\}$, $\phi = 90°$; (f) $\mathrm{Im}\{A_{33}\}$, $\phi = 90°$; (g) $\mathrm{Re}\{A_{33}\}$, $\phi = 180°$; (h) $\mathrm{Im}\{A_{33}\}$, $\phi = 180°$: ——, asymptotic result (101); – – –, numerical summation.

those of Figure 4. The sharp peaks evident at the low frequencies are due to the $O(1/(\alpha_1 a)^5)$ terms, neglected in the asymptotic evaluation, which are not negligible at the low frequencies when compared to the small $O(1)$ term which is, however, the leading order term. This interpretation was confirmed by increasing the value of the exterior fluid density, which resulted in the numerical result agreeing with the asymptotic result. For these angles,

the real part of A_{23} is small on the same scale and is neglected here. For $\theta = 90^\circ$, $A_{23}(\alpha, \phi)$ is identically zero. As an example of the case when P and Q are approximately real, Figure 7 shows the real and imaginary parts of $A_{23}(\alpha, \phi)$ for $\theta = 80^\circ$ and $\phi = 30$ and 90°. In this case the real and imaginary parts are of comparable magnitude, and the levels are higher than those of Figure 6. There is good agreement between the asymptotic approximation and the numerical evaluation at all the frequencies shown, although at the very low frequencies (< 50 Hz) there is some slight evidence of the $O(1/(\alpha_1 a)^5)$ terms in the numerical result.

Figure 8 shows the real part of $A_{33}(\alpha, \phi)$ for $\theta = 45^\circ$, $\phi = 0$, 30, 90 and 180°. The imaginary part is negligible, except for peaks in the numerical result corresponding to peaks in the real part. It is not presented here. The asymptotic results in Figure 8 are typical of those for which P and Q are approximately imaginary, cf., Figure 4. As in Figure 6, at the low frequencies the numerical result shows sharp peaks which are due to the $O(1/(\alpha_1 a)^5)$ terms neglected in the leading order asymptotic evaluation which may nevertheless be large compared to the leading order term which is $O(1)$, if $\alpha_1 a$ is not sufficiently large. Figure 9 shows both the real and imaginary parts of $A_{33}(\alpha, \phi)$ for $\theta = 90^\circ$, $\phi = 0$, 30, 90 and 180°. The real and imaginary parts are of comparable magnitudes. The agreement between the asymptotic and numerical evaluations is good, although again at the low frequencies the numerical result exhibits some sharp peaks which are neglected in the leading order asymptotic approximation. For these angles P and Q are approximately real, but the peaks in both the real and imaginary parts of A_{33} are much smoother than the corresponding peaks of A_{22} in Figure 5 and A_{23} in Figure 7.

5. CONCLUSIONS

The usual method for calculating the displacement of an infinite elastic cylindrical shell involves expanding all the displacements as series of circumferential harmonics. Here a method for evaluating the sum of these harmonics in the asymptotic limit of heavy exterior fluid-loading has been presented. It results in simple expressions involving only trigonometric functions for the displacement components when the shell is excited by a line force, either at the force application point, or elsewhere on the shell circumference. The numerical examples presented here show that these asymptotic approximations exhibit excellent agreement with results obtained by summing a large number of circumferential harmonics, over a wide frequency range. Thus, these simpler expressions may be used instead of performing the harmonic expansion which may require many terms. In addition, the dependence on the parameters of the shell and fluid is made explicit in expressions (45), (58), (69), (71), (83), (90), (92), (94) and (101) allowing the straightforward interpretation of the results, and their application to problems involving line constraints.

REFERENCES

1. J. E. GREENSPON 1960 *Journal of Sound and Vibration* **32**, 571–578. Vibrations of a thick-walled cylindrical shell—comparison of the exact theory with approximate theories.
2. G. B. WARBURTON 1961 *Journal of Mechanical Engineering Science* **3**, 69–79. Vibrations of a cylindrical shell in an acoustic medium.
3. C. R. FULLER and F. J. FAHY 1982 *Journal of Sound and Vibration* **81**, 501–518. Characteristics of wave propagation and energy distributions in cylindrical elastic shells filled with fluid.
4. C. R. FULLER 1983 *Journal of Sound and Vibration* **87**, 409–427. The input mobility of an infinite circular cylindrical shell filled with fluid.
5. J. F. M. SCOTT 1988 *Journal of Sound and Vibration* **125**, 241–280. The free modes of propagation of an infinite fluid-loaded thin cylindrical shell.

6. F. G. LEPPINGTON 1978 *Journal of Sound and Vibration* **58**, 319–332. Acoustic scattering by membranes and plates with line constraints.
7. B. R. MACE 1980 *Journal of Sound and Vibration* **73**, 487–504. Periodically stiffened fluid-loaded plates, II: response to line and point forces.
8. G.-F. LIN and J. M. GARRELICK 1977 *Journal of Sound and Vibration* **61**, 1014–1018. Sound transmission through periodically framed parallel plates.
9. E. A. SKELTON 1990 *Proceedings of the Royal Society of London* **A427**, 401–418. Acoustic scattering by parallel plates with a single connector.
10. I. D. WILKEN and W. SOEDEL 1976 *Journal of Sound and Vibration* **44**, 563–576. The receptance method applied to ring-stiffened cylinders: analysis and modal characteristics.
11. D. J. MEAD and N. S. BARDELL 1987 *Journal of Sound and Vibration* **115**, 499–520. Free vibration of a thin cylindrical shell with periodic circumferential stiffeners.
12. E. A. SKELTON 1993 *Journal of Sound and Vibration* **148**, 243–264. Acoustic scattering by a disc constraining an infinite fluid-loaded cylindrical shell.
13. E. S. REDDY and A. K. MALLIK 1985 *Journal of Sound and Vibration* **103**, 519–531. Response of and sound radiation from a layered cylinder with regular axial stiffeners.
14. D. J. MEAD and N. S. BARDELL 1986 *Journal of Sound and Vibration* **111**, 229–250. Free vibration of a thin cylindrical shell with discrete axial stiffeners.
15. J. BJARNASON, J. D. ACHENBACH and T. IGUSA 1992 *Wave Motion* **15**, 23–41. Acoustic radiation from a cylindrical shell with an internal plate.
16. Y. P. GUO 1992 *Journal of the Acoustical Society of America* **91**, 926–938. Sound scattering from an internally loaded cylindrical shell.
17. Y. P. GUO 1993 *Journal of the Acoustical Society of America* **93**, 1936–1946. Sound scattering from cylindrical shells with internal elastic plates.
18. Y. P. GUO and L. B. FELSEN 1993 *Journal of the Acoustical Society of America* **94**, 896–899. Wave-number spectrum and normal-mode solutions for sound-scattering from internally loaded cylindrical shells.
19. Y. P. GUO 1996 *Journal of the Acoustical Society of America* **99**, 1495–1505. Acoustic radiation from cylindrical shells due to internal forcing.
20. Y. P. GUO 1996 *Journal of the Acoustical Society of America* **99**, 2701–2713. Acoustic scattering from cylindrical shells with deck-type internal plate at oblique incidence.
21. A. BAILLARD, J. M. CONOIR, D. DECULTOT, G. MAZE, A. KLAUSON and J. METSAVEER 2000 *Journal of the Acoustical Society of America* **107**, 3208–3216. Acoustic scattering from fluid-loaded stiffened cylindrical shell: Analysis using elasticity theory.
22. M. C. JUNGER and D. FEIT 1972 *Sound, Structures and their Interaction*. Cambridge, Massachusetts: MIT Press.
23. M. ABRAMOWITZ and I. A. STEGUN 1972 *Handbook of Mathematical Functions*. National Bureau of Standards, United States Department of Commerce, Washington, DC.
24. D. S. JONES 1966 *Generalised Functions*. London: McGraw-Hill.
25. I. S. GRADSHTEYN and I. M. RYZHIK 1980 *Tables of Integrals, Series and Products*. New York: Academic Press.